J. of KOSOMBE
Vol. 19, No. 6, 585-593, 1998

Using Bayesian Approaches to Reduce Truncation Artifact in Magnetic Resonance Imaging

S.J. Lee

Department of Electronic Engineering, Paichai University
(Received August 14, 1998, Accepted December 10, 1998)

요 약 : 퓨리에 자기공명영상 기법의 경우 촬영시간 단축 및 적절한 신호대잡음비 유지를 위해 phase-encoded 신호의 개수를 감소시키는 경우가 종종 있다. 그러나, 이는 재구성된 영상에 번짐과 물결무늬 형태의 truncation artifact를 초래한다. 본 논문에서는 이러한 truncation artifact를 감소시키기 위해 Bayesian 방법에 근거한 새로운 정칙화기법을 제안한다. Truncation artifact는 phase 방향으로만 형성되므로 종전의 상호 대칭형태의 주변화소를 고려한 piecewise smoothness 사전정보를 사용할 경우 read 방향으로의 미세한 영상정보가 유실되기 쉽다. 따라서, 본 연구에서는 종전의 단순대칭형 보다 개선된 형태로서 자기공명영상의 공간정보를 포착할 수 있는 정교한 사전정보의 형태를 제안한다. 본 연구진의 실험결과 새롭게 제안된 방법을 적용할 경우 truncation artifact가 감소될 뿐 아니라 종전의 미세정보유실 현상이 감소됨으로써 tissue regularity와 경계가 한층 더 향상됨을 확인할 수 있었다.

Abstract : In Fourier magnetic resonance imaging (MRI), the number of phase encoded signals is often reduced to minimize the duration of the studies and maintain adequate signal-to-noise ratio. However, this results in the well-known truncation artifact, whose effect manifests itself as blurring and ringing in the image domain. In this paper, we propose a new regularization method in the context of a Bayesian framework to reduce truncation artifact. Since the truncation artifact appears in the phase direction only, the use of conventional piecewise-smoothness constraints with symmetric neighbors may result in the loss of small details and soft edge structures in the read direction. Here, we propose more elaborate forms of constraints than the conventional piecewise-smoothness constraints, which can capture actual spatial information about the MR images. Our experimental results indicate that the proposed method not only reduces the truncation artifact, but also improves tissue regularity and boundary definition without oversmoothing soft edge regions.
Key words : Magnetic Resonance Imaging, Truncation Artifact, Bayesian Methods, Gibbs Distribution, Deterministic Annealing

INTRODUCTION

In magnetic resonance (MR) imaging, the numerical value of each pixel in the image reflects the intensity of the MR signal, which is determined by the density of the resonating nuclei and by two chemical parameters called the *longitudinal relaxation time* T_1 and *spin-spin relaxation time* T_2[1]. Spatially-resolved information from those parameters can be encoded in the measured data in a variety of ways. After more than a decade of evolution in data acquisition strategies (pulse sequences), the Fourier-encoding scheme has become most popular.

이 논문은 1997년 한국학술진흥재단의 공모과제 (1997-002-200173) 연구비에 의하여 연구되었음.
통신저자 : 이수진, (302-735) 대전시 서구 도마 2동 439-6
배재대학교 전자공학과,
Tel. (042)520-5711, Fax. (042)520-5663

In conventional Fourier imaging, such as spin-echo and inversion recovery, the nuclei in the image slice are selectively "excited" by the application of a frequency-selective pulse in the presence of a field gradient perpendicular to the imaging plane. The bandwidth of the radio-frequency (RF) pulse and the strength of the gradient field (G_z) determine the slice thickness. In order to resolve the signal amplitude in the 2-D Fourier space (k-space), the application of G_z is followed by the two additional periods - "phase encoding" and "readout". During the phase-encoding period, a gradient G_y on the imaging plane is applied and causes the nuclei to precess at characteristic frequencies of their location with respect to the y coordinate. The readout period is to acquire the signal in the presence of another gradient G_x on the imaging plane, which is perpendicular to G_y. Depending on the location of the nuclei with respect to

x, the nuclei resonate at characteristic frequencies determined by the strength of G_x.

Although the signal obtained from the three periods (excitation, phase encoding, and readout) contains information from all voxels in the imaging slice, the information is not sufficient to determine the signal amplitude required in each voxel to reconstruct an image. Therefore, in order to fill in the 2-D Fourier space (k_x, k_y) in a rectilinear fashion, the cycle of the three periods has to be "repeated" with a different setting of the phase-encoding gradient G_y. For a 256 $\times$256 matrix, for example, the required number of cycles is 256; the 256 *free induction decay* signals, each corresponding to a different value of the phase-encoding gradient G_y, have to be sampled 256 times. In practice, the number of phase-encoded signals is often reduced to minimize the acquisition time and maintain adequate signal-to-noise ratio. Unfortunately, however, reduction of the number of phase-encoded signals results in the well-known "truncation artifact" or "Gibbs oscillations" when the truncated k-space data are Fourier transformed to reconstruct the image[2,3].

The purpose of this study is to reduce the truncation artifact and improve the quality of MR images. A number of methods to reduce the truncation artifact in MR images have been proposed in the literature[4-7]. Some of the methods[5] use a version of the Papoulis-Gerchberg algorithm[8,9] and show some good results, but its convergence may be questionable[10]. Sebastiani and Barone[7] proposed a regularization method in the context of a Bayesian framework. Their motivation of using a Bayesian approach was based on the fact that the reconstruction with incomplete k-space data is an ill-posed problem. In their model, the prior information employed was derived from the assumption that the true image could be described by a piecewise constant model with no ramps or smooth edges. Although this type of constraint may be useful for reduction of truncation artifact in the phase direction, the use of piecewise constant models with symmetric neighbors may degrade the small details or soft edge regions in the read direction.

In this paper, we propose an improved Bayesian method with more elaborate forms of priors than the conventional piecewise constant priors, which can not only reduce the truncation artifact in the phase direction, but also retain the soft edge regions in the read direction.

Bayesian Models for Magnetic Resonance Images

In this paper we model the image on a 2-D finite discrete lattice indexed by (i,j). Uppercase bold quantities denote 2-D random fields and corresponding uppercase italicized quantities denote random variables. Similarly, lowercase bold quantities denote 2-D vector fields and corresponding lowercase, italicized quantities denote the elements of the vector field. For example, $\Pr(\mathbf{F}=\mathbf{f})$ denotes the probability that the random field $\mathbf{F}$ takes the value $\mathbf{f}$, and F_{ij} and f_{ij} denote elements of $\mathbf{F}$ and $\mathbf{f}$ at the location (i,j), respectively.

The Bayesian approach consists of two components - the likelihood and the prior. The likelihood is a probabilistic description of the stochastic processes that relate the original unknown data $\mathbf{F}$ to the observed measurements $\mathbf{G}$. The prior is a probabilistic description of the assumptions on the underlying image $\mathbf{F}$. In a Bayesian approach, these two probabilities are combined to yield *a posteriori* probability via Bayes' Theorem:

$$\Pr(\mathbf{F}=\mathbf{f} \mid \mathbf{G}=\mathbf{g}) = \frac{\Pr(\mathbf{G}=\mathbf{g} \mid \mathbf{F}=\mathbf{f})\Pr(\mathbf{F}=\mathbf{f})}{\Pr(\mathbf{G}=\mathbf{g})}, \qquad (1)$$

where $\Pr(\mathbf{G}=\mathbf{g} \mid \mathbf{F}=\mathbf{f})$ is the likelihood probability, $\Pr(\mathbf{F}=\mathbf{f})$ the prior probability. Since the elements of $\mathbf{g}$ are the observed measurements, $\Pr(\mathbf{G}=\mathbf{g})$ is simply a number. In the case of MR images, the observed image $\mathbf{g}$ is the magnitude of the 2-D Fourier transform of the raw data, and the underlying image $\mathbf{f}$ corresponds to the magnitude of the transverse magnetization.

For MR images, random errors in the real and imaginary parts of each pixel are described by independent Gaussian distributions with identical standard deviation[11]. Moreover, pixel intensities in a magnitude image are well approximated by a Gaussian distribution[12]. Therefore, the likelihood, $\Pr(\mathbf{G}=\mathbf{g} \mid \mathbf{F}=\mathbf{f})$, is expressed as a product of independent Gaussian distributions:

$$\Pr(\mathbf{G}=\mathbf{g} \mid \mathbf{F}=\mathbf{f}) = \prod_{ij} \exp\left[-\frac{(f_{ij}-g_{ij})^2}{2\sigma^2}\right] \qquad (2)$$

where σ is the standard deviation of the observed magnitude image, which can be known by measuring values in a background region. In fact, the standard deviations of real and imaginary parts are very close to each other so that a unique σ can be assumed[7]. The likelihood in (2) measures

the closeness of the solution **f** to the observed image **g**.

In our context, priors are probabilistic descriptions of the spatial character of the underlying image. A popular means of modeling the prior distribution is to use the Gibbs distribution which is given by

$$\Pr(\mathbf{F}=\mathbf{f})=\frac{1}{Z}\exp(-\lambda E_p(\mathbf{f})), \tag{3}$$

where λ is a constant, Z and E_P are the normalizing constant (partition function) and the "energy function" for smoothness constraints, respectively. Since the Gibbs distribution has a Markovian property, prior distributions modeled as a Gibbs distribution can be specified in terms of the probability distribution of a pixel conditioned on only its nearby pixels, rather than through the joint distribution on random variables associated with the entire object.

In designing priors, it is common to choose the energy functions which penalize pixel configurations with large intensity gradient within each neighbor. However, it is often important to model priors that can locate and preserve the discontinuities that bound smooth regions such as anatomical regions. Geman and Geman[13] introduced the powerful idea of including unobservable "line processes" in the image model in order to preserve discontinuities in the image. The line processes are binary variables (0 or 1) that act to suspend smoothness constraints at sites where they are turned on ($l=1$). A horizontal line process at location (i,j), $l_{ij}^h=1$, indicates a horizontal edge (discontinuity between pixels along the vertical direction) and a vertical line process, $l_{ij}^v=1$, indicates a vertical edge (discontinuity along the horizontal direction).

Versions of the line processes have been proposed for medical imaging as well as the surface reconstruction problem in computer vision[13-15]. In particular, Blake and Zisserman[16] proposed mechanical analogs to regularizers in which a class of "piecewise smoothness" constraints derived from properties of ideal physical materials were used as models in the associated surface reconstruction problem. The representative mechanical models are the "weak membrane" and the "weak plate". These priors are defined over the pixel intensities and the line processes. The corresponding energies are

$$E_p(\mathbf{f},\mathbf{l})=\sum_{ij}\left[f_v^2(i,j)(1-l_{ij}^h)+f_h^2(i,j)(1-l_{ij}^v)\right]+\alpha\sum_{ij}\left(l_{ij}^h+l_{ij}^v\right) \tag{4}$$

for weak membrane (WM), and

$$E_p(\mathbf{f},\mathbf{l})=\sum_{ij}\left[f_{vv}^2(i,j)+2f_{hv}^2(i,j)+f_{hh}^2(i,j)\right](1-l_{ij})+\alpha\sum_{ij}l_{ij} \tag{5}$$

for weak plate (WP). In (4) f_v and f_h denote the discrete first order derivatives in the vertical and the horizontal directions, respectively, $f_{vv}(i,j)$ and $f_{hh}(i,j)$ in (5) the discrete second partial derivatives in the vertical and horizontal directions, respectively, and $f_{hv}(i,j)$ the second partial cross derivative. The last term α in both (4) and (5) is a positive constant. The first and second partial derivative terms in (4) and (5) are the membrane and the thin plate [16,17], respectively, which encourage smoothness except where discontinuities ($l=0$) occur. One might set $l=1$ at all locations to minimize energy, but the last term penalizes the creation of the discontinuities, charging in amount of α each discontinuity. Due to its nature in favoring piecewise constant reconstructions, the WM prior has the unfortunate effect of turning a ramp into a single step or stepped terraces depending on the slope of the ramp region, which is known as the "gradient limit" effect [16]. The interpretation of the WP energy in (5) is similar to that of the WM energy except that the WP encourages smoothness even in ramplike regions without incurring a penalty. That is, a "crease", a discontinuity in first derivative, will turn on the line process. Thus the discontinuities in the WP correspond to discontinuities in the intensity gradient in addition to those in the pixel intensity itself. The details on the properties of WM and WP and their applications can be found in [16,15].

Sebastiani and Barone [7] used a version of the WM prior to reduce truncation artifact in MR images. In their work the prior model was chosen on the assumption that the true MR image could be described by a piecewise constant model with no ramps or smooth edges. In fact, the use of WM that favors piecewise constant reconstructions is quite useful for suppressing the Gibbs oscillations in the presence of noise. However, close inspection of a typical brain MR image and its profile plot shown in Fig. 1 reveals that many regions in the brain MR image are far from piecewise constant. Therefore, the use of WM may result in the generation of spurious edges due to its gradient limit effect, as well as the loss of the details for soft edges due to its tendency to favor piecewise flat reconstructions.

Unlike the WM which has the fundamental limitation of

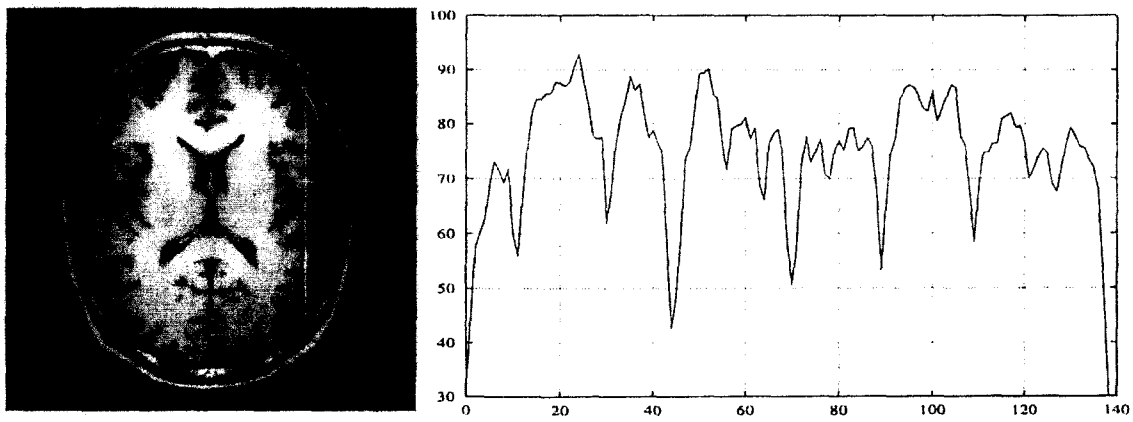

Fig. 1. A T_1-weighted brain MR image and a profile plot. (a) A T_1-weighted brain MR image (256×256) reconstructed by the FFT with 256 phase-encoding steps. (T_R=500ms, T_E=13ms, field of view (FOV)=24cm, thickness=5mm, gap=2.5mm). The raw data were acquired twice and averaged to reduce noise. (b) A profile plot along the vertical line in (a)

turning a ramp into stepped terraces, the WP has no such limit. This is one of the major benefits of using a higher order scheme [15]. However, care must be taken when the WP model is used to reduce truncation artifact in MR images; the ringing artifact reveals ramplike regions which may not be suppressed well by the WP model due to its tendency to favor piecewise ramplike reconstructions.

In most clinical MR imaging, the direction of the phase-encoding gradient is usually determined to avoid any possible contamination of diagnostic content due to *motion* artifacts since the motion during data acquisition produces undesirable "ghost" artifacts, which appear as periodic replications of moving anatomic structures in the phase direction[18]. For brain axial images, in particular, the phase-encoding gradient is usually in the horizontal direction when the object is oriented as shown in Fig. 1. This is done mainly to avoid artifacts due to the eyeball motion and the blood flow in middle cerebral arteries, which may degrade the important diagnostic content of the images when the phase gradient is in the vertical direction. Therefore, we argue here that more elaborate forms of priors that can not only reduce the truncation artifact in the phase direction, but also preserve ramplike regions in the read direction.

One possible modification of the prior model for the above argument may then be a mixture of the WM and the WP, where the WM is used for reducing the ringing artifact in the phase direction and the WP for preserving ramplike structures in the read direction. The corresponding new prior energy is given by

$$E_P(\mathbf{f},\mathbf{l}) = \sum_{ij}\left[f_{vv}^2(i,j)(1-l_{ij}^h)+f_h^2(i,j)(1-l_{ij}^v)\right] + \alpha_h\sum_{ij} l_{ij}^h + \alpha_v\sum_{ij} l_{ij}^v, \quad (6)$$

where α_h and α_v are positive constants that penalize creating discontinuities in the horizontal and vertical directions, respectively. Note that, in our new *hybrid* model, the horizontal direction is described by the WM and the vertical direction by the WP; the WM suppresses truncation artifact as well as noise in the horizontal (phase) direction, and the WP restores ramplike structures in the vertical (read) direction. One could also consider a linear combination of the WM and the WP by adding (4) and (5). Due to the gradient limit behavior of the WM, however, the linear combination turns out to perform poorly in reconstruction problems [16].

Maximum *A Posteriori* Estimation

We have shown in the previous section that the Bayesian approach combines the likelihood and the prior to yield *a posteriori* probability via Bayes' Theorem. Since our new prior model include the unobservable binary variables **l**, we may rewrite Bayes' Theorem with the aid of the line processes:

$$\Pr(\mathbf{F}=\mathbf{f},\ \mathbf{L}=\mathbf{l}\mid \mathbf{G}=\mathbf{g}) = \frac{\Pr(\mathbf{G}=\mathbf{g}\mid \mathbf{F}=\mathbf{f},\ \mathbf{L}=\mathbf{l})\ \Pr(\mathbf{F}=\mathbf{f},\ \mathbf{L}=\mathbf{l})}{\Pr(\mathbf{G}=\mathbf{g})}, \quad (7)$$

where $\mathbf{l}$ is the line process and $\mathbf{L}$ is the associated 2-D random field. One possible approach is then to estimate both $\mathbf{f}$ and $\mathbf{l}$ using the well-known maximum *a posteriori* (MAP) approach:

$$(\hat{\mathbf{f}}, \hat{\mathbf{l}}) = \arg\max_{(\mathbf{f},\mathbf{l})} \Pr(\mathbf{F}=\mathbf{f}, \mathbf{L}=\mathbf{l} \mid \mathbf{G}=\mathbf{g})$$

$$= \arg\max_{(\mathbf{f},\mathbf{l})} [-\log\Pr(\mathbf{G}=\mathbf{g} \mid \mathbf{F}=\mathbf{f}) - \log\Pr(\mathbf{F}=\mathbf{f}, \mathbf{L}=\mathbf{l})] \tag{8}$$

From (2), (3), (6), and (8), the MAP estimate becomes the minimization of the following overall energy function, $E(\mathbf{f}, \mathbf{l})$:

$$E(\mathbf{f}, \mathbf{l}) \overset{\text{def}}{=} E_L(\mathbf{f}) + \lambda E_P(\mathbf{f}, \mathbf{l})$$

$$= \frac{1}{2\sigma^2}\sum_{ij}(f_{ij}-g_{ij})^2 + \lambda\Big\{\sum_{ij}[f_{vv}^2(i,j)(1-l_{ij}^h) + f_h^2(i,j)(1-l_{ij}^v)] + \alpha_h\sum_{ij} l_{ij}^h + \alpha_v\sum_{ij} l_{ij}^v\Big\} \tag{9}$$

where $E_L(\mathbf{f}) \overset{\text{def}}{=} \frac{1}{\sigma^2}\sum_{ij}(f_{ij}-g_{ij})^2$ is the likelihood energy. In (9) λ is identified as the *hyperparameter* that weights the prior respect to the likelihood; as λ increases, the degree of the prior influence increases.

The MAP estimate for this problem is to minimize the overall energy function in (9). Unfortunately, however, the overall energy may have numerous stable states, each corresponding to a local minimum of the energy due to the weak continuity constraints on the prior energy. To overcome this problem, an optimization method that has an ability to "jump out" of a local minimum is necessary. Although the well-known simulated annealing method is guaranteed to find the global minimum, the amount of computation required is intractable as reported in[7]. In this work, we use a deterministic annealing algorithm based on the continuation method[19,15], where the energy function is approached by a sequence of energy functions indexed by a parameter β. The sequence is obtained by transformation of the probability distributions (3) to

$$P_\beta(\mathbf{Y}=\mathbf{y} \mid \mathbf{X}=\mathbf{x}) = \frac{1}{Z(\mathbf{x};\beta)}\exp(-\beta E(\mathbf{y})), \tag{10}$$

When the probability distributions for the likelihood and the prior are transformed to the form of (10), the corresponding posterior distribution is given by

$$\Pr_\beta(\mathbf{F}=\mathbf{f}, \mathbf{L}=\mathbf{l} \mid \mathbf{G}=\mathbf{g}) = \frac{1}{Z(\mathbf{g};\beta)}\exp[-\beta\{E_L(\mathbf{f}) + \lambda E_P(\mathbf{f},\mathbf{l})\}], \tag{11}$$

where $Z(\mathbf{g};\beta)$ is the partition function parametrized by β. Note that the line process can be eliminated from the posterior distribution in (11) by integrating out the line process and resulting in the "marginal" posterior, which is given by

$$\Pr_\beta(\mathbf{F}=\mathbf{f} \mid \mathbf{G}=\mathbf{g}) = \sum_{\{\mathbf{l}\}}\Pr_\beta(\mathbf{F}=\mathbf{f}, \mathbf{L}=\mathbf{l} \mid \mathbf{G}=\mathbf{g}) = \frac{1}{Z_M(\mathbf{g};\beta)}\exp[-\beta E_L(\mathbf{f})]\sum_{\{l_{ij}\}_{ij}}\exp[-\beta\lambda E_P(\mathbf{f},\mathbf{l})], \tag{12}$$

where $Z_M(\mathbf{g};\beta)$ is the partition function for the marginal posterior, the notation $\sum_{\{l_{ij}\}}$ refers to summation over all possible realizations of the binary field $\mathbf{l}$, and

$$\sum_{\{l_{ij}\}_{ij}}\exp[-\beta\lambda E_P(\mathbf{f},\mathbf{l})] = \sum_{\{l_{ij}\}_{ij}}\exp\Big[-\beta\lambda\Big(\sum_{ij}[f_{vv}^2(i,j)(1-l_{ij}^h) + f_h^2(i,j)(1-l_{ij}^v)] + \alpha_h\sum_{ij} l_{ij}^v + \alpha_v\sum_{ij} l_{ij}^v\Big)\Big]$$

$$= \prod_{ij}\sum_{\{l_{ij}\}_{ij}}\exp[-\beta\lambda\{f_{vv}^2(i,j)(1-l_{ij}^h) + \alpha_h l_{ij}^h\}]\exp[-\beta\lambda\{f_h^2(i,j)(1-l_{ij}^v) + \alpha_v l_{ij}^v\}]$$

$$= \prod_{ij}(\exp[-\beta\lambda f_{vv}^2(i,j)] + \exp[-\beta\lambda\alpha_h])(\exp[-\beta\lambda f_h^2(i,j)] + \exp[-\beta\lambda\alpha_v])$$

$$= \exp\Big[\sum_{ij}\log(\exp[-\beta\lambda f_{vv}^2(i,j)] + \exp[-\beta\lambda\alpha_h]) + \sum_{ij}\log(\exp[-\beta\lambda f_h^2(i,j)] + \exp[-\beta\lambda\alpha_v])\Big].$$

Therefore, the marginal posterior is given by

$$\Pr_\beta(\mathbf{F}=\mathbf{f} \mid \mathbf{G}=\mathbf{g}) = \frac{1}{Z_M(\mathbf{g};\beta)}\exp[-\beta\{E_L(\mathbf{f}) + \lambda E_{MP}(\mathbf{f};\beta)\}],$$

where

$$E_{MP}(\mathbf{f};\beta) \overset{\text{def}}{=} -\frac{1}{\beta\lambda}\Big[\sum_{ij}\log(\exp[-\beta\lambda f_{vv}^2(i,j)] + \exp[-\beta\lambda\alpha_h]) + \sum_{ij}\log(\exp[-\beta\lambda f_h^2(i,j)] + \exp[-\beta\lambda\alpha_v])\Big] \tag{13}$$

The above equation is identified as the marginal prior energy. Notice that, at large values of β, if $\alpha > x$, where x

refers to either $f_{vv}^2(i,j)$ or $f_h^2(i,j)$ and α refers to either α_h or α_v, the first term inside the log(·) expression dominates and the entire expression reduces to x. If $\alpha < x$, the second term inside the log(·) expression dominates and the entire expression reduces to α. Inspection reveals that $E_{MP}(\mathbf{f};\beta)$ at large β is in fact equivalent to $E_P(\mathbf{f}, \mathbf{I})$ in (6). The details on the continuation method can be found in[19,15].

Our task now reduces to finding the minimum at a given β of the following energy function:

$$E(\mathbf{f};\beta) = E_L(\mathbf{f}) + \lambda E_{MP}(\mathbf{f};\beta).$$

For the optimization method, one can use gradient descent method. However, closed-form solution for f_{ij} that minimizes the above objective function cannot be directly obtained by setting $\frac{\partial E(\mathbf{f};\beta)}{\partial f_{ij}}=0$, as the differentiation results in an expression transcendental in f_{ij}. One possible solution to this problem is to consider the transcendental term to be a new, albeit dependent on f_{ij}, variable and to descend on each such variable separately[14]. We define the transcendental terms as

$$z_{ij}^{v} \overset{\text{def}}{=} \frac{1}{1+\exp[-\beta\lambda(f_h^2(i,j)-\alpha_v)]}$$
$$z_{ij}^{h} \overset{\text{def}}{=} \frac{1}{1+\exp[-\beta\lambda(f_{vv}^2(i,j)-\alpha_h)]} \quad (14)$$

Using the new variables in (14), a corresponding objective function, $M(\mathbf{f},\mathbf{z};\beta) \overset{\text{def}}{=} \sigma^2 E(\mathbf{f},\mathbf{z};\beta)$, becomes

$$M(\mathbf{f},\mathbf{z};\beta)=\frac{1}{2}\sum_{ij}(f_{ij}-g_{ij})^2+\sigma^2\lambda\sum_{ij}\{f_{vv}^2(i,j)(1-z_{ij}^{h}) + f_h^2(i,j)(1-z_{ij}^{v})+\alpha_h z_{ij}^{h}+\alpha_v z_{ij}^{v}\}+K(z). \quad (15)$$

where $K(z)$ is the term that does not involve f_{ij}. The update equation for f_{ij} for gradient descent method can now be obtained by the following equation:

$$\frac{f_{ij}^{k+1}-f_{ij}^{k}}{\gamma} = -\frac{\partial M(\mathbf{f}^k, \mathbf{z}^k;\beta)}{\partial f_{ij}^{k}},$$

where the superscript k denotes the index associated with the step of the algorithm, and γ is the step size. The update equation for f_{ij} is given by

$$f_{ij}^{k+1}=f_{ij}^{k}-\gamma[(f_{ij}-g_{ij})-2\sigma^2\lambda\{(f_{ij+1}-f_{ij})(1-z_{ij}^{v}) +2(f_{i+1j}-2f_{ij}+f_{i-1j})(1-z_{ij}^{v}) -(f_{ij}-f_{ij-1})(1-z_{ij-1}^{v}) -(f_{ij}-2f_{i-1j}+f_{i-2j})(1-z_{i-1j}^{h}) -(f_{i+2j}-2f_{i+1j}+f_{ij})(1-z_{i+1j}^{h})\}]^k,$$

where $[\cdot]^k$ denotes the kth step of the algorithm. To complete the definition of the algorithm, we may specify the two stopping criteria and an annealing schedule. The annealing schedule specifies the rule for changing β at each epoch. Iterations at a given β are performed until the relative energy change $\frac{E_k - E_{k-1}}{E_k - E_0}$, where k indexes iteration number within an epoch, is less than a threshold. The entire simulation is terminated when $\mathbf{z} \le \tau$ or $\mathbf{z} \ge 1-\tau$, where τ is chosen as a threshold. This is based on the fact that the approach of $\mathbf{z}$ to either 0 or 1 corresponds to the approach of (13) to (6).

Experimental Results

In order to demonstrate the practical utility of our new method, we acquired brain MR data from a healthy volunteer using a 1.5T GE Signa (Horizon Echo Speed) MRI system. Pulse sequences used in the experiments were conventional spin-echo sequences with T_R = 500ms, T_E = 30ms for T_1-weighted images, T_R = 2000ms, T_{E_1} = 30ms and T_{E_2} = 80ms for proton-density and T_2-weighted images, respectively. Each sequence was employed to collect 10 transverse slices with the following parameters: thickness=5mm, gap =2.5mm, FOV=21cm. The orientations for the phase and read gradients were horizontal and vertical directions, respectively. In this paper, we report the results from T_1- and T_2-weighted images only for one slice.

Figures 2(a) and 3(a) show 256×256 brain axial in T_1- and T_2-weighted images, respectively, reconstructed by the fast Fourier transform (FFT) of 256×256 measured k-space data. In order to see the effect of truncation artifact, we chose a certain number of columns in the k-space data and filled in the remaining columns with zeros. Figure 2(b) shows a T_1-weighted 256×256 image reconstructed with only 116 columns of the raw data. Similarly, Fig. 3(b) shows a T_2-weighted 256×256 image reconstructed with only 96 columns of the raw data. Notice that the Gibbs oscillations are clearly visible and the spatial resolution is degraded.

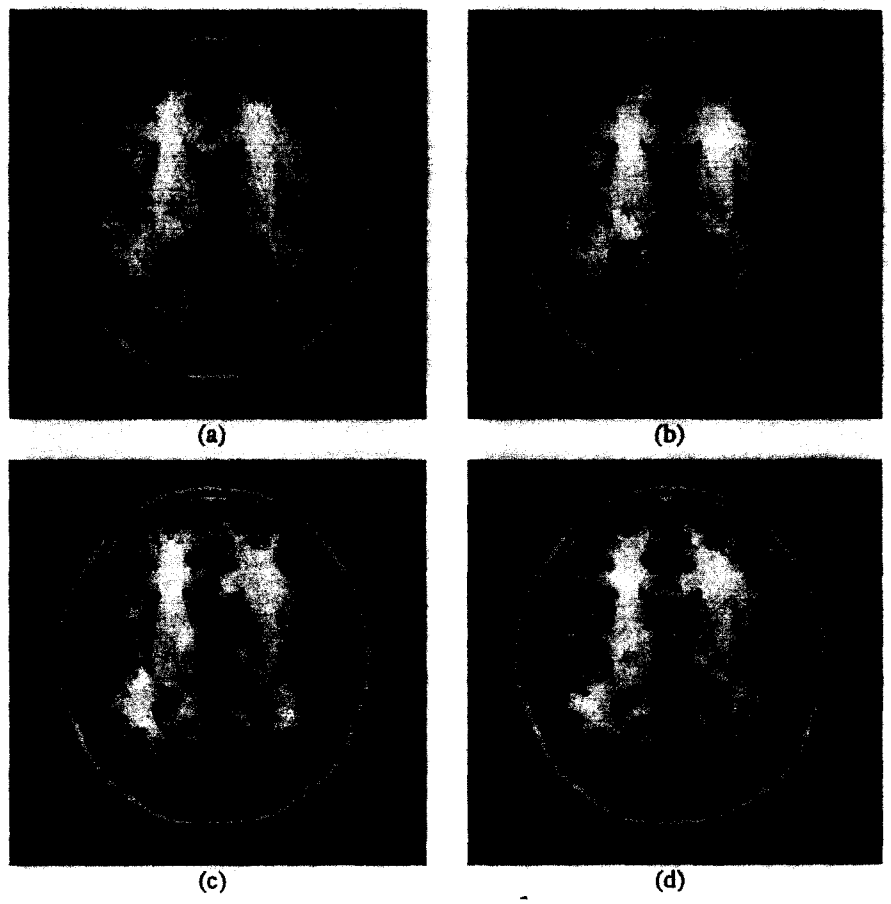

Fig. 2. Reduction of truncation artifact in T_1-weighted images. (a) A T_1-weighted brain MR image(256×256) reconstructed with 256×256 measured k-space data. (b) Reconstruction by FFT with only 116 columns of k-space data. (c) Reduction of truncation artifact using the MAP approach with WM prior. (d) Reduction of truncation artifact using the MAP approach with hybrid prior

To test and compare the performance of our new prior model - the hybrid model - with the WM model, we implemented the proposed method on a SUN UltraSparc 170 I workstation. A problem with Bayesian methods, including our own models, is that it is difficult to set hyperparameters (λ and α in our case) automatically. While this is an area of active research, for the present work we set these values empirically. We first chose the parameter value of λ by considering the degree of smoothness in the reconstructed images; the λ was adjusted to smooth out both the Gibbs oscillations and the noise. The gradient limit effects were also considered in finding the value of λ for the WM model. In the experiments, we used one value of λ for both prior models. Having set the λ, we adjusted the parameter α for the WM model empirically to preserve grey/white matter and tissue boundaries, and used the value of α for α_v in the hybrid model. The parameter α_h was also adjusted to preserve tissue regularity and smooth edges along the read (vertical) direction. The annealing schedule ran through 22 values with a doubling at each new value of β starting from $\beta=0.125$. With a constant initial estimate for $\mathbf{f}$, the initial value for the parameter β was chosen to be small enough to yield a very smooth initial reconstruction. Iterations at a given β may be performed until the relative energy change is less than a threshold. However, in order to allow a sufficient number of iterations at a given β, we fixed the iteration number to 50. The entire procedure was terminated using a threshold value of $\tau = 0.1$. The initial condition for $\mathbf{f}$ was a constant intensity of 1.0 and $\mathbf{z}$ was initialized to 0.5. The total computation time for 22 different values of β was approximately 2 minutes.

Figure 2(c) shows the result obtained by applying the weak-membrane model in (4) to the T_1-weighted image with truncation artifact in Fig. 2(b). Notice that, although the truncation artifact is reduced remarkably, the result looks artificially patchy and most of the smooth edges are

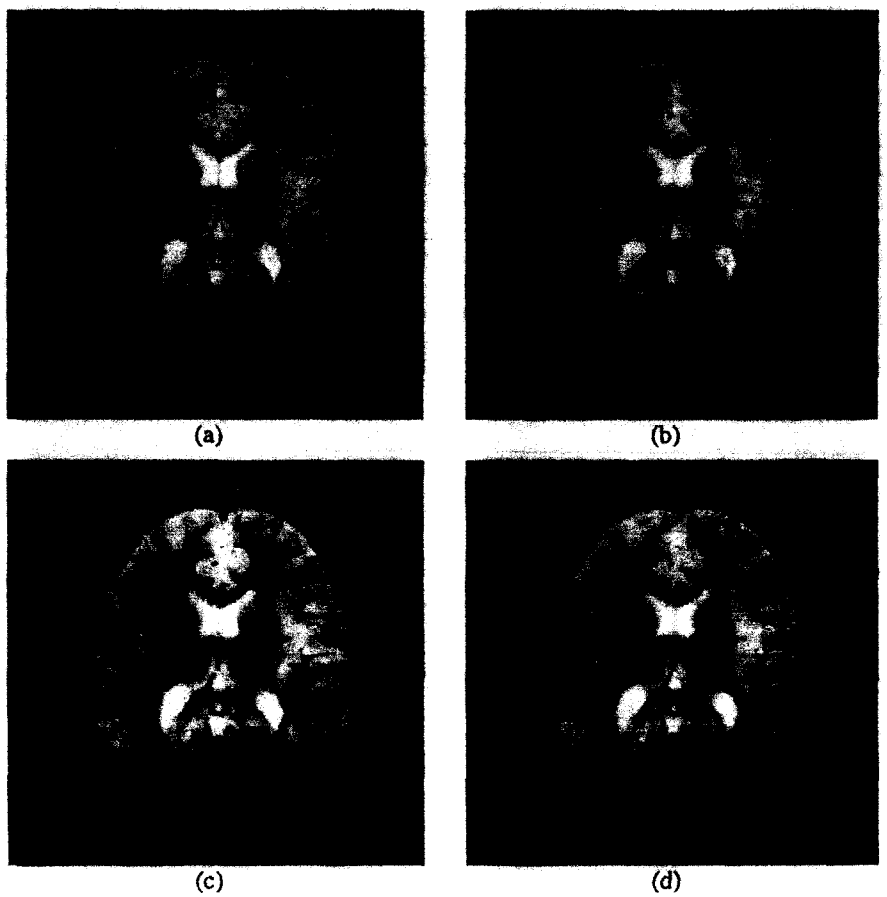

Fig. 3. Reduction of truncation artifact in T_2-weighted images. (a) A T_2-weighted brain MR image(256×256) reconstructed with 256×256 measured k-space data. (b) Reconstruction by FFT with only 96 columns of k-space data. (c) Reduction of truncation artifact using the MAP approach with WM prior. (d) Reduction of truncation artifact using the MAP approach with hybrid prior

lost, a result not unexpected since WM tends to favor piecewise constant reconstructions. The patchiness due to the gradient limit effects may be reduced by increasing λ, but then a tradeoff results and the details in small areas are lost due to excessive smoothness. The weak membrane attempts to create step edges even in the ramp regions in the read (vertical) direction, resulting in spurious discontinuities. On the other hand, the extension of the WM model in the read direction to a higher-order model using (6) reduces the artifice of WM reconstruction as seen in Fig. 2 (d). Comparison of Fig. 2(d) to (c) shows that the hybrid model reduces truncation artifact as well as noise without introducing spurious discontinuities in the read direction. While the visual improvements from Fig. 2(c) to (d) are not stunning, close inspection reveals that the result obtained by applying the hybrid model, in fact, enhances tissue regularity and boundaries without oversmoothing the soft edge regions, and captures subtle aspects of the brain structure in Fig. 2(a). Figures 3(c) and (d) show the results obtained by applying the weak membrane and the hybrid models, respectively, to the T_2-weighted image with truncation artifact in Fig. 3(b). Again, the result from the hybrid model in Fig. 3(d) reduces truncation artifact as well as noise with no ill effects when compared to the result from the WM model in Fig. 3(c).

Summary and Conclusion

We have considered a new, improved method for reduction of truncation artifact in magnetic resonance imaging. The approach taken in this work is related to other efforts [7] in which Gibbs priors in the context of a Bayesian framework were used to reflect the local spatial structure of true image. Unlike other imaging modalities, however, the MR images contain ringing artifacts, when reconstructed with truncated data, which appear in only one of the

two spatial directions. Therefore, the use of conventional piecewise-constant models, which apply equally to both directions, can oversmooth important anatomical structure in the other direction. In contrast, the hybrid model proposed in this paper is an extension of the weak membrane to a higher-order model in one direction to preserve ramplike structures that occur occasionally in that direction. Our experimental results show that the hybrid model not only reduces the truncation artifact in the phase direction but also enhances tissue regularity and boundaries without degrading the smooth edges in the read direction.

Another improvement in this work is to use deterministic annealing to optimize non-convex objective functions. The deterministic annealing algorithm used in our experiments dramatically reduces the computational cost compared to the well-known simulated annealing and provides good solutions. Therefore, the parallel implementation of deterministic algorithm, in conjunction with the development of a systematic way of determining hyperparameters, will make our method more practical in its clinical applications.

REFERENCES

1. Z.-H. Cho, J.P. Jones, and M. Singh, *Foundation of Medical Imaging*, John Wiley & Sons, Inc., New York, NY, 1993.
2. M.L. Wood and R.M. Hankelman, "*Truncation Artifacts in Magnetic Resonance Imaging*", *J. Magn. Reson. Med.*, 2, pp. 517-526, Dec. 1985.
3. R.M. Henkelman and M.J. Bronskill, "*Artifacts in Magnetic Resonance Imaging*", *Rev. Magn. Reson. Med.*, 2, pp. 1, 1986.
4. R.T. Constable and R.M. Henkelman, "*Data Extrapolation for Truncation Artifact Removal*", *Magn. Reson. Med.*, 17, pp. 108-118, 1986.
5. X. Hu and A.E. Stillman, "*Technique for Reduction of Truncation Artifact in Chemical Shift Images*", *IEEE Trans. Med.* Imaging, MI-16, pp. 290-294, Sep. 1991.
6. P. Barone and G. Sebastiani, "*A New Method of Magnetic Resonance Image Reconstruction with Short Acquisition Time and Truncation Artifact Reduction*", *IEEE Trans. Med. Imaging*, MI-11, pp. 250-259, Jun. 1992.
7. G. Sebastiani and P. Barone, "*Truncation Artifact Reduction in Magnetic Resonance Imaging by Markov Random Field Methods*", *IEEE Trans. Med. Imaging*, MI-14, pp. 434-441, sep. 1995.
8. R.W. Gerchberg, "*Super-Resolution through Error Energy Reduction*", *Optica Acta*, 21(9), pp. 709-720, 1974.
9. A. Papoulis, "*A New Algorithm in Spectral Analysis and Band-Limited Extrapolation*", *IEEE Trans. Circuits Syst.*, CAS-22(9), pp. 735-742, 1975.
10. S.K. Plevritis and A. Macovski, "*Spectral Extrapolation of Spatially Bounded Images*", *IEEE Trans. Med. Imaging*, MI-14, pp. 487-497, Sep. 1991.
11. R.M. Henkelman, "*Measurement of Signal Intensities in the Presence of Noise in MR Images*", *Med. Phys.*, 12(2), pp. 232-233, 1985.
12. G.M. Jenkins and D.G. Watts, *Spectral Analysis and its Applications*, Holden-Day, San Francisco, 1968.
13. S. Geman and D. Geman, "*Stochastic Relaxation, Gibbs Distributions and the Bayesian Restoration of Images*", *IEEE Trans. Patt. Anal. Mach. Intel.*, PAMI-6(6), pp. 721-741, Nov. 1984.
14. D. Geiger and F. Girosi, "*Parallel and Deterministic Algorithms from MRFs: Surface Reconstruction*", *IEEE Trans. Patt. Anal. Mach. Intel.*, PAMI-13(5), pp. 401-412, May 1991.
15. S.J. Lee, A. Rangarajan, and G. Gindi, "*Bayesian Image Reconstruction in SPECT Using Higher Order Mechanical Models as Priors*", *IEEE Trans. Med. Imaging*, MI-14(4), pp. 669-680, Dec. 1995.
16. A. Blake and A. Zisserman, *Visual Reconstruction, Artificial Intelligence*, MIT Press, Cambridge, MA, 1987.
17. S.J. Lee, I.T. Hsiao, and G.R. Gindi, "*The Thin Plate as a Regularizer in Bayesian SPECT Reconstruction*", *IEEE Trans. Nucl. Sci.*, NS-44(3), pp. 1381-1387, Jun. 1997.
18. D.D. Stark and W.G. Bradley, *Magnetic Resonance Imaging*, pp. 145-164, Mosby-Year Book, St. Louis, 1992.
19. A. Rangarajan, M. Lee, G. Zubal, and G. Gindi, "*A Continuation Method for Emission Tomography*", *In Proc. IEEE Nuclear Science Symposium and Medical Imaging Conference*, vol. 2, pp. 1204-1207, Oct. 1992.